The 15th International Symposium on Magnetic Bearings, August 3-6, 2016, Mojiko Hotel, Kitakyushu, Japan

ISMB15

Homopolar-biased Hysteresis Bearingless Slice Motors

Minkyun NOH*, Wolfgang GRUBER** and David L. TRUMPER*

* Department of Mechanical Engineering, Massachusetts Institute of Technology
77 Massachusetts Avenue, Cambridge, MA 02139, USA
E-mail: minkyun@mit.edu, trumper@mit.edu

** Institute of Electrical Drives and Power Electronics, Johannes Kepler University
Altenberger Straße 69, 4040 Linz, Austria
E-mail: wolfgang.gruber@jku.at

Abstract

We present a new concept of bearingless slice motors that levitates and rotates a ring-shaped rotor made of a semi-hard magnetic material such as D2 steel. The rotor is biased with a homopolar permanent-magnetic flux, on which 2-pole flux can be superimposed to generate suspension forces. The torque is generated by a hysteretic coupling between the rotor and a rotating 6-pole stator field. We discuss the design of the prototype system and its performance estimates from FEA simulations.

Key words : Hysteresis motors, Homopolar bearingless motors, Flux-biased magnetic bearings, Slice motors.

1. Introduction

Bearingless motors, or self-bearing motors, levitate and drive a rotor with a single stator unit, and therefore can eliminate mechanical bearings in a compact form factor. Since 1980s, bearingless motor technology has drawn international research efforts, which led to developments of bearingless motors of various types (Chiba et al., 2005). Some applications, such as blood pumps and pumps for high-purity chemical processes, find bearingless motors especially usefull. Bearingless slice motors, developed by Barletta et al. (1996) and further studied by Silber et al. (2005), are particularly suitable for these applications; they levitate the pump impeller passively in the axial and tilting directions and actively in the two radial directions. The passive levitation is realized with the reluctance forces between a soft-magnetic stator and an impeller comprising a permanent magnet, whereas active levitation is realized with a feedback control. Gruber et al. (2015) developed a bearingless slice motor that drives a reluctance rotor. Here, the magnet is eliminated from the rotor and placed on the stator to create a homopolar bias flux.

In this paper, we present a new concept of bearingless slice motors using a hysteresis rotor. Replacing the reluctance ring in (Gruber et al., 2015) with a hysteresis ring enables the advantages from bearingless hysteresis motors: robust and simple rotor construction as well as smooth torque generation. These advantages make our new bearingless motor suitable for high-speed rotary applications and for ultraclean pumping systems or blood pumps that require disposable impeller replacement. Bearingless hysteresis motors were first conceptualized and realized by Imani-Nejad et al. (2014), and further studied by Zhou et al. (2014) in application to a satellite attitude control. Our key contribution building upon these previous works is the incorporation of homopolar flux biasing for decoupling the force and torque generations, force generation independent of the rotor position, higher force/current for suspension, and suspension force linearization. These benefits originate from the similarity in magnetic structure to flux-biased magnetic bearings studied by Studer (1977) and Allaire et al. (1992), and homopolar/hybrid bearingless motors studied by Ichikawa et al. (2001).

2. Operating principle

The operating principle of a homopolar hysteresis bearingless motor can be best understood as a combination of a flux-biased magnetic bearing and a hysteresis motor. We first revisit the force generation mechanism of a flux-biased magnetic bearing as applied to our stator/rotor design. Next, we discuss hysteresis torque generation by superposing an additional 6-pole rotating magnetic flux.

2.1. Force generation

Figure 1 schematically shows a cross-sectional side view of the motor. Here, the stator comprising twelve outer L-shaped teeth and an inner central flux-biasing structure forms an annular space for a hysteresis rotor. The homopolar bias flux (dashed blue lines) from the permanent magnet traverses through the hysteresis rotor radially outwards and returns via the stator bottom plate. The stator coils can superpose a 2-pole suspension flux (solid red lines) on the bias flux to generate a radial force in the x direction. Another 2-pole suspension flux can be applied for y axis suspension. Assuming the hysteresis effect is negligible in the radial direction, the force generation mechanism becomes similar to those of flux-biased magnetic bearings studied by Studer (1977) and Allaire et al. (1992): The supperimposed 2-pole suspension flux is added to the homopolar flux on the positive x direction, and substracted from the homopolar flux on the negative x direction, thereby generating a differential magnetic force on the rotor. The strength of the flux can be regulated based on the position measurement for stable suspension. Due to the homopolar bias flux, other degrees of freedom, displacement along z axis and tilts about x and y axes, are passively stable.

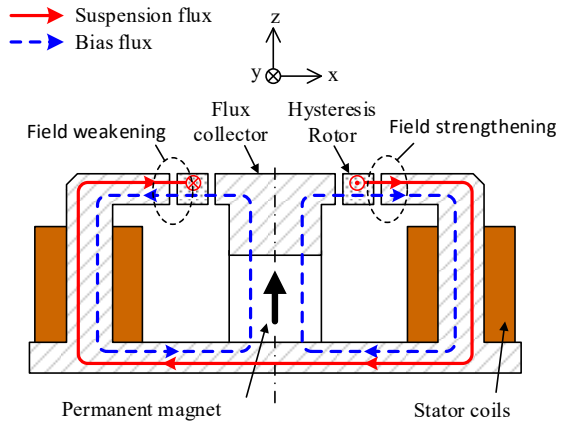

Fig. 1 Cross-sectional side view. The dashed blue lines represent the permanent-magnetic bias flux, and the red lines represent the suspension flux.

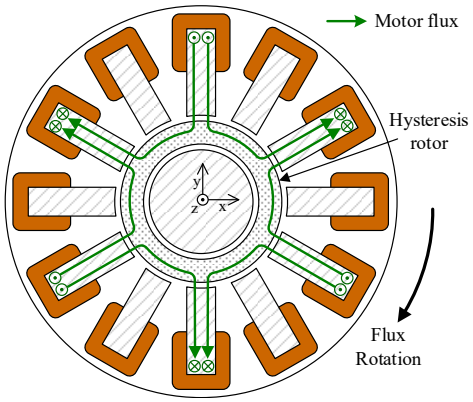

Fig. 2 Top view showing the rotating flux distribution to generate torque.

2.2. Torque generation

The torque generation mechanism of hysteresis motors is first studied by Teare (1940). Figure 2 illustrates the action of a hysteresis motor in our design. As the stator generates a rotating 6-pole motor flux (solid green lines), the rotor becomes magnetized with a 6-pole pattern. Because of the hysteresis, the induced magnetization tends to be persistent on the rotor and lag behind the stator excitation by some angle. The interaction between the excitation magnetic fields and the induced magnetization generates a torque

$$\tau = \frac{V P_{torque}}{4\pi} \oint B_\theta \, dH_\theta \tag{1}$$

for sufficiently thin rings, where V is the material volume, P_{torque} is the number of poles of the motor flux, H_θ is the tangential component of the magnetic field intensity, and B_θ is the tangential component of the magnetic flux density (Teare, 1940). The integral is evaluated along the circumference of the rotor.

The 6-pole motor flux ($P_{torque} = 6$) does not generate radial forces by interacting with either of the homopolar bias flux ($P_{bias} = 0$) and the 2-pole suspension flux ($P_{force} = 2$). This is because the 6-pole motor flux does not satisfy the necessary condition to generate radial forces, $P_2 = P_1 \pm 2$ (Chiba, 2005), with the other sets of flux. The principle says that in order to generate suspension forces for a given flux distribution of P_1 number of poles, we should superimpose an additional flux pattern of P_2 number of poles such that $P_2 = P_1 \pm 2$. Specifically in our case, $P_{torque} \neq P_{force} \pm 2$, $P_{torque} \neq P_{bias} \pm 2$, and $P_{force} = P_{bias} + 2$. Therefore, the superposition of the homopolar bias flux ($P_{bias} = 0$) and the suspension flux ($P_{force} = 2$) is the mechanism for force generation.

Also, the homopolar bias flux and the 2-pole suspension flux does not generate a significant drag torque. This is because when the rotor is stabilized at the center, the variation of the bias flux and suspension flux along the circumference becomes negligible, therby generating a negligible eddy-current drag. Thus, the mechanisms for torque generation and suspension force generation are in principle decoupled in this design.

3. Prototype system design

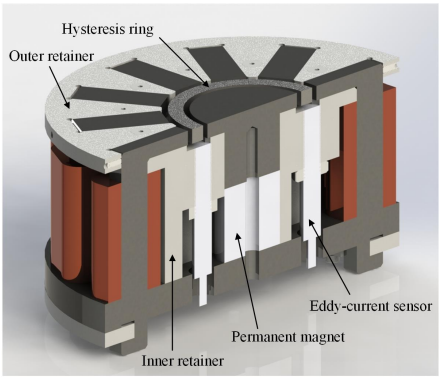

Fig. 3 3D rendering (cut-away side view) of the prototype motor.

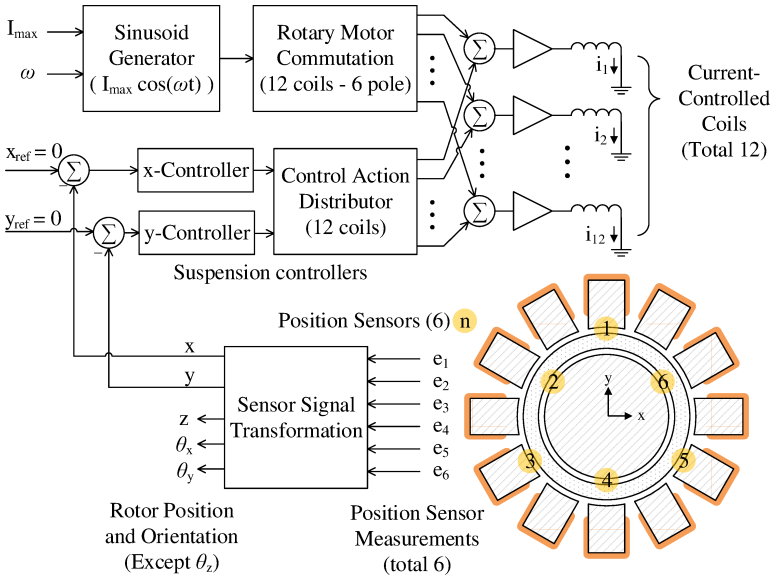

Fig. 4 Block diagram for the control system.

The 3D rendering of the prototype system is shown in Fig. 3. A hysteresis ring of 55-mm outer diameter, 45-mm inner diameter, and 5-mm height is made with D2 steel. The D2 steel is a semi-hard magnetic material that has been successfully used in (Imani-Nejad et al., 2014) and (Zhou et al., 2014). A NeFeB permanent magnet of 25.4-mm outer diameter, 12.7-mm inner diameter, and 25.4-mm height is used for the homopolar bias flux. The stator teeth and bottom plate are made with laminated steel sheets of 0.5–mm thickness, machined via wire-electrical discharge machining (wire-EDM). Each stator tooth has a concentrated coil of 0.5-mm thickness and 800-turns. Key design parameters of the prototype system is summarized in Table 1.

Table 1 Design parameters.

	Parameter	Value
D_o	Rotor outer diameter	55 mm
D_i	Rotor inner diameter	45 mm
g_0	Air gaps (in/out)	2 mm
B_{bias}	Bias flux density	0.3 T

Table 2 Performance estimates.

	Parameter	Value
k_r	Radial stiffness	-8.56 N/mm
k_z	Axial stiffness	1.96 N/mm
k_ϕ	Tilting stiffness	0.55 Nm/rad
K_i	Force constant	16 N/A
τ_z	Hysteresis torque	2.25 mNm

Figure 4 shows the block diagram for the control system. Six eddy current sensors (LDC 1000 from Texas Instruments) are used to estimate the radial displacements of the rotor, which are fed back to the suspension controllers for active levitation. A total of 12 current-controlled linear power amplifiers, which were used in (Imani-Nejad et al., 2014), drive the 12 coils individually. The amplifiers are tuned for a bandwidth of 5 kHz, and a DC gain of 200 mA/V. The flux superposition happens inside the controller by superposing current commands to the bank of power amplifiers. As for the real-time controller, we use a cRIO-9076 target from National Instruments.

4. Simulation result

The stator is designed based on the results from magnetostatic ANSYS Maxwell simulations, such that the rotor axial stiffness is predicted to be $k_z = 1.96$ N/mm, open-loop radial stiffness is $k_r = -8.56$ N/mm, and tilting stiffness is $k_\phi = 0.55$ Nm/rad. Figure 5 shows the relation between the suspension forces and magneto-motive forces (MMF) as computed in an ANSYS Maxwell simulation. The hysteresis of D2 steel is not considered for the simulation; instead, the normal magnetization curve, a single-valued curve connecting the tips of minor hysteresis loops, is used for the simulation.

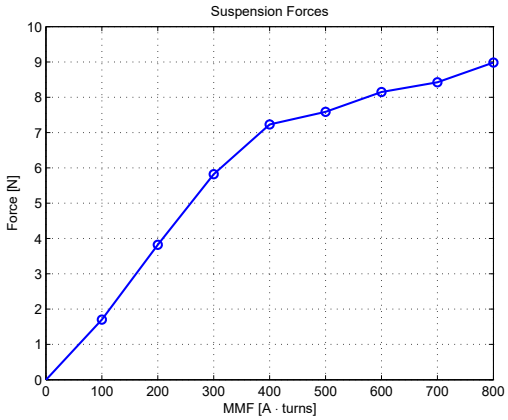

Fig. 5 The relation between the suspention forces and the magnetomotive forces (MMF). Three adjacent coils on one side are driven with the same polarity of MMF, and the three adjacent coils on the oposite side are driven with the opposite polarity of MMF.

For the suspension force simulation, three adjacent coils on one side are driven with the same polarity of MMF, and the three adjacent coils on the oposite side are driven with the opposite polarity of MMF. With the number of turns for each coil being $N = 800$, the force constant is computed as K_i =16 N/A in the linear range. The non-linearity out of this range is due to saturation of the stator iron.

Figure 6 shows how the tangential flux density is distributed in the middle of the rotor along the circumferential direction. The parameter θ_e is the electrical angle, which we vary as $\theta_e = \omega_e t$ to generate a traveling flux wave by the stator coils. The data for Fig. 6 are from a simulation case where the stator is energized with a six-pole traveling MMF of 500 amp turns peak amplitude. The resulting tangential flux densities in the rotor resemble sinusoids with an amplitude of 0.7 T. The hysteresis torque estimate for this simulation case can be computed from Eq. (1) as the integral is evaluated using the experimentally measured B-H loop data shown in Figure 7. Here, the solid red line is for the case where the flux density is sinusoidal with a peak amplitude of 0.7 T. The loop area of this case is approximately 1200 A/m·T, which leads to a hysteresis torque estimate of τ_z =2.25 mNm.

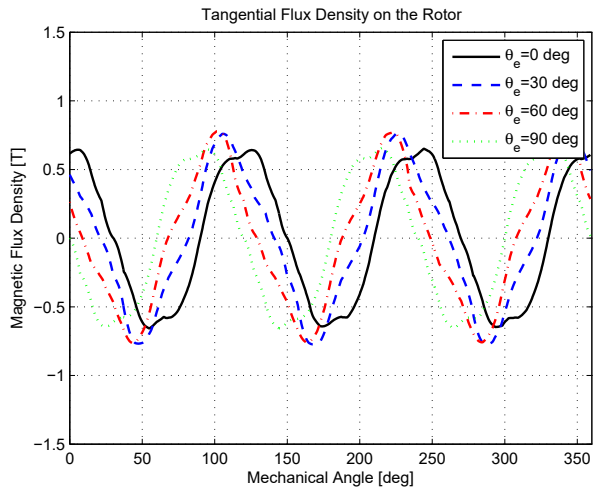

Fig. 6 Tangential flux density distribution in the rotor along the circumference. The parameter θ_e is the electrical angle.

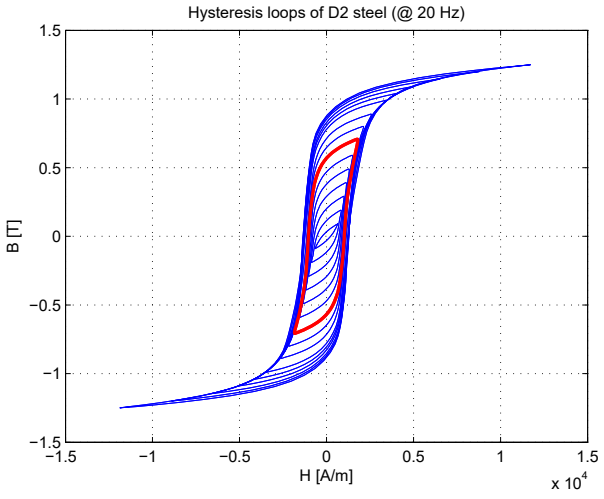

Fig. 7 B-H hysteresis loops of D2 steel measured at 20 Hz following IEC 60404-6 international standard. The D2 steel sample was in the same geometry as the rotor. The solid red line is for the case where the flux density is sinusoid with an amplitude of 0.7 T.

5. Conclusions

In this paper, we presented a new concept of bearingless motor that is based on a homopolar flux-biased magnetic

bearing for force generation and a hysteresis motor for torque generation. FEA simulations were performed on the prototype design in order to obtain estimates of key performance values such as radial/axial/tilting stifnesses and force constant. These values will be used to design a feedback controller for rotor levitation. Currently we are building the first prototype system, and expect to experimentally validate the concept in the near future.

6. Acknowledgements

The authors thank National Instuments for donation of the controller hardware used in this research.

References

Allaire, P. E., Maslen, E. H., Humphris, R. R., Sortore, C. K. and Studer, P. A., Low Power Magnetic Bearing Design for High Speed Rotating Machinery, International Symposium on Magnetic Suspension Technology (1992), Part 1, pp.317-329.

Barletta, N. and Schöb, R. Design of a Bearingless Blood Pump, International Symposium on Magnetic Suspension Technology (1996), Part 1, pp.265-274.

Chiba, A. , Fukao, T., Ichikawa, O., Oshima, M., Takemoto, M. and Dorrell,D. G., Magnetic Bearings and Bearingless Drives, ELSEVIER, 2005.

Gruber, W., Rothböck, M. and Schöb, R., Design of a Novel Homopolar Bearingless Slice Motor With Reluctance Rotor, IEEE Transactions on Industry Applications, Vol.51, No.2 (2015), pp.1456-1464.

Ichikawa, O., Chiba, A. and Fukao, T., Inherently Decoupled Magnetic Suspension in Homopolar-type Bearingless Motors, IEEE Transactions on Industry Applications, Vol.37, No.6 (2001), pp.1668-1674.

Imani-Nejad, M. and Trumper, D. L., Hysteresis Self-bearing Motor, Proceedings of ISMB14 (2014), pp. 737-742.

Silber, S., Amrhein, W., Bösch, P., Schöb, R. and Barletta, N., Design Aspects of Bearingless Slice Motors, IEEE/ASME Transactions on Mechatronics, Vol.10, No.6 (2005), pp.611-617.

Studer, P., A Practical Magnetic Bearing, IEEE Transactions on Magnetics, Vol.13, No.5 (1977), pp.1155-1157.

Teare, B. R., Theory of hysteresis-motor torque, AIEE Transactions, Vol.59, No.12 (1940), pp.907912.

Zhou, L., Imani-Nejad, M. and Trumper, D. L., Magnetically Suspended Reaction Sphere with One-axis Hysteresis Drive, Proceedings of ISMB14 (2014).